

Molecular Dynamics Simulation of Folding and Diffusion of Proteins in Nanopores

Leili Javidpour,^a Muhammad Sahimi,^{b,†} and M. Reza Rahimi Tabar^{a,c}

^a*Dep. of Physics, Sharif University of Technology, Tehran 11365, Iran*

^b*Mork Family Department of Chemical Engineering & Materials Science, University of Southern California, Los Angeles, California 90089-1211, USA*

^c*CNRS UMR 6529, Observatoire de la Côte d'Azur, BP 4229, 06304 Nice Cedex 4, France*

A novel combination of discontinuous molecular dynamics and the Langevin equation, together with an intermediate-resolution model, are used to carry out long (several μs) simulation and study folding transition and transport of proteins in slit nanopores. Both attractive (U^+) and repulsive (U^-) interaction potentials between the proteins and the pore walls are considered. Near the folding temperature T_f and in the presence of U^+ the proteins undergo a repeating sequence of folding/partially-folding/ unfolding transitions, while T_f decreases with decreasing pore sizes. The opposite is true when U^- is present. The proteins' effective diffusivity D is computed as a function of their length (number of the amino acid groups), temperature T , the pore size, and the interaction potentials U^\pm . Far from T_f , D increases (roughly) linearly with T , but due to the thermal fluctuations and their effect on the proteins' structure near T_f , the dependence of D on T in this region is nonlinear. Under certain conditions, transport of proteins in smaller pores can be *faster* than that in larger pores.

PACS: 87.15.Aa, 83.10.Mj, 87.15.Cc, 87.15.Vv, 87.83.+a

Proteins' importance to biological systems cannot be overstated [1]: as enzymes they catalyze and regulate cells' activities; tissues are made of proteins, while as antibodies proteins are a vital part of the immune system. Proteins with globular structure fold into compact and biologically active configurations, and an important problem is understanding the mechanisms by which they attain their folded structure, and factors that contribute to the folding [2–4]. Such understanding is important due to debilitating illnesses, such as Alzheimer's and Parkinson's diseases, that are believed to be the result of accumulation of toxic protein aggregates [5–8], as well as to the industrial production of enzymes and therapeutic proteins based on the DNA recombinant method [9].

While the three-dimensional (3D) structure of native proteins is controlled by their amino acid sequence [2–4], their transport properties and the kinetics of their folding depend on the local environment. But, whereas protein folding in dilute solutions under bulk condition, typically used in *in vitro* studies, is relatively well-understood, the more important problem of protein folding in a confined medium is not. The environment inside a cell in which proteins fold is crowded, with the volume fraction of the crowding agents (such as RNA) may be 0.2-0.3. Thus, even in the absence of interactions between proteins and other cellular molecules, their movement inside the cell is limited. The limitation affects proteins' stability. Experiments indicated [10] that confinement often stabilizes the proteins' native structure [11], denatures them in the limited space of the cage model, first suggested by Anfinsen [2–4], and *accelerates* folding relative to that in bulk solutions. Studies of proteins of different native architectures in cylindrical nanopores indicated [12] that,

in vivo folding is *not* always spontaneous; rather, a subset of proteins may require molecular chaperones.

Protein (enzyme) immobilization using porous solid support, via adsorption, encapsulation, and covalent linking, has been used for a long time [13, 14]. Such practical applications as biocatalysis [15] and biosensors also entail not only better understanding of the folding in confined media, but also transport of proteins in such media. At the same time, protein purification using nanoporous membranes is also gaining attention [16]. SiC nanoporous membranes [17] allow [18] diffusion of proteins up to 29000 Daltons, but exclude larger ones. Despite the fundamental and practical significance of transport of protein in confined media, there is currently little understanding of the phenomenon.

The goal of this paper is twofold. First, we use molecular dynamics (MD) simulation to study protein folding and stability in slit nanopores. Second, we utilize a novel combination of MD simulation and the Langevin equation (LE) to study protein transport in the nanopores. To our knowledge, our combination of the MD simulation and the LE has never been proposed before, nor has there been any simulation of transport of proteins in nanopores. For such important practical applications as membrane purification, biocatalysis, and sensors, the transport of proteins in nanopores is of utmost importance. A slit nanopore is a reasonable model for the type of pores that one encounters in such applications [15–18] and, despite its simplicity, it might also be a reasonable model for the pores in biological membranes.

Some Monte Carlo [19] and MD [5, 20] simulations of proteins' behavior in nanopores were reported before. In particular, Lu *et al.* [5] and Cheung *et al.* [20] studied

folding of proteins in *spherical* pores of different radii. Cheung *et al.* studied the phenomenon as a function of the volume fraction of a crowding agent, which they modeled by a bed of hard spheres with repulsive interaction with the proteins. While a spherical pore may be a suitable model for the cavity of GroEl-GroES complex, it is not so for the pores of membranes, biocatalysts, and sensors that are of prime interest to us. Instead, the slit (and cylindrical) pores are more appropriate. Moreover, for the types of applications that we consider, the pore space consists of interconnected channels, which is completely different from what Refs. [5,20] considered.

In addition, the protein model that we use (see below) is, in our opinion, much more realistic than what the previous investigations [5, 20] utilized. For example, they used a simplified model for the amino acids that was based on two united atom (UA) beads. Moreover, the side chains of the amino-acid residues were not explicitly considered. The model that we utilize represents the amino acids using four UA beads (see below), while the side chains are also considered explicitly, hence honoring the proteins' structure much more realistically.

We simulate de novo-designed α family of proteins [21], which consists of only 4 types of amino acids in their 16-residue sequence, simplified further [22] to a sequence of hydrophobic (H) and polar (P) residues. Using periodicity in the H-P sequence of the 16-residue peptide α_{1B} , we made 3 other sequences with lengths $\ell = 9, 23$ and 30 residues. As the four proteins have similar native structures, the differences in their behavior is attributed to their lengths. The simulations indicated that they all fold into an α -helix.

The proteins are modeled by an intermediate-resolution model [23–26], with several changes described below. Every amino acid is represented by four UA groups or beads. A nitrogen UA represents the amide N and hydrogen of an amino acid, a C_α UA represents the α -C and its H, and a C UA for the carbonyl C and O. The fourth bead R represents the side chains, all of which are assumed to have the same diameter as CH_3 . All the backbone bond lengths and bond angles are fixed at their ideal values, and the distance between consecutive C_α UA is fixed according to experimental data.

To carry out long and efficient simulations, we use discontinuous MD (DMD) [27]. This allowed us to carry out 5 μ s MD simulations, one order of magnitude longer than the previous simulations. The forces acting on the beads are the excluded-volume effect, and attraction between bonded and pseudobonded beads, between pairs of backbone beads during HB formation, and between hydrophobic side chains. Nearest-neighbor beads along the chain backbone are covalently bonded, as are the C_α and R UAs. Pseudobonds are between next-nearest neighbor beads along the backbone to keep the backbone angles fixed; between neighboring pairs of C_α beads to maintain their distances close to the experimental data, and

between side chains and backbone N and C UAs to hold the side-chain beads fixed relative to the backbone. All of this keep the interpeptide group in the *trans* configuration, and all the residues as L -isomers, as required.

The potential U_{ij} between a pair ij of bonded beads, separated by a distance r_{ij} , is given by, $U_{ij} = \infty$, for, $r_{ij} \leq l(1 - \delta)$, and $r_{ij} \geq l(1 + \delta)$, and, $U_{ij} = 0$ for $l(1 - \delta) < r_{ij} < l(1 + \delta)$. Here, l is the ideal bond length, and $\delta = 0.02375$ is the tolerance in the bond's length [23–26]. The hydrophobic (HP) interactions between the side chains and the H in the sequence, if there are at least 3 intervening residues between them, is given by, $U_{HP} = \infty, -\epsilon_{HP}$, and 0 for, $r_{ij} \leq \sigma_{HP}$, $\sigma_{HP} < r_{ij} \leq 1.5\sigma_{HP}$, and $r_{ij} > 1.5\sigma_{HP}$, respectively, where σ_{HP} is the HP side-chains' diameter.

The HB interaction may occur between the N and C beads with at least 3 intervening residues, but each bead may not contribute to more than one HB at any time, with the range of the interaction being about 4.2 Å. The HBs are stable when the angles in N-H-O and C-O-H, controlled by a repulsive interaction between each of the N and C beads with the neighboring beads of the other one, are almost 180°. Thus, if a HB is formed between beads N_i and C_j , a repulsive interaction between neighbor beads of N_i , namely, C_{i-1} and $C_{\alpha i}$, with C_j is assumed, and similarly for the neighbor beads of C_j , namely, N_{j+1} and $C_{\alpha j}$, with the N_i bead.

An N or C bead at one end of the protein has only one neighbor bead in its backbone, instead of 2. Hence, controlling the HB angles will be limited, causing the HBs with one of their terminal constituents to be less restricted and, thus, more stable than the other HBs. This may cause formation of non- α -helical HBs in a part of the protein between the N and C beads, and of semistable structures that influence the results. To address this problem, assume that the N-terminal bead, N_1 , has a HB with C_j . For $i = 1$, bead C_{i-1} does not exist to have a repulsive interaction with C_j and help control the HB angles. So, we use $C_{\alpha 1}$. Not only can we consider the repulsion between this bead and C_j , but also we define an upper limit for their distance so as to control the motion freedom of N_1 and C_j that constitute the beads in the HB. The potential U_{kl} of such interactions is given by, $U_{kl} = \infty, \epsilon_{HB}$, 0, and ∞ for $r_{kl} \leq \frac{1}{2}(\sigma_k + \sigma_l)$, $\frac{1}{2}(\sigma_k + \sigma_l) < r_{kl} \leq d_1$, $d_1 < r_{kl} \leq d_2$, and, $r_{kl} > d_2$, respectively.

Two H atoms have chemical bonds with the nitrogen in the proteins' N-terminal, and are free to rotate around the N_1 - $C_{\alpha 1}$ bond, while at the same time satisfying the constraints on the angles between the chemical bonds of N_1 . Thus, if a HB is formed, one of the two H atoms lies in the plane of N, O and C, such that the angles in N-H-O and C-O-H are as close to 180° as possible. Hence, we force the maximum distance between $C_{\alpha 1}$ and C_j to be the same as the maximum distance d_2 between $C_{\alpha i}$ and C_j in the usual HBs, and similarly when the C-

terminal C_ℓ has a HB with N_i . This allows us to control the angles in a HB that contains N_1 . The T -dependence (T is dimensionless) of d_2 (in \AA), obtained from separate MD simulations (the details will be given elsewhere), is, $d_2 \simeq 5.53 - 0.019/T$ for N_1 - $C_{\alpha j}$, and $d_2 \simeq 5.69 - 0.044/T$ for C_ℓ - $C_{\alpha i}$.

There is also hard-core repulsion between two unbonded beads that have no HB and HP interactions. At the same time, interactions between a pair of beads, separated along the chain by 3 or fewer bonds, are more accurately represented by those between the atoms themselves, not the UAs. Thus, we developed a variant of the previous models [23–26] to account for such interactions: the beads are allowed to overlap by up to 25% of their bead diameters, while for those separated by 4 bead diameters the allowed overlap is 15% of their diameters.

We use a slit nanopore, modeled as the space between two 2D structureless carbon walls in the xy plane between $z = \pm h/2$, with periodic boundary conditions in the x and y directions. The interaction between the walls and the protein beads is, $U_{PW} = \infty, -\epsilon_{PW}, 0, -\epsilon_{PW},$ and ∞ for, $z_X \leq -(h/2 - d_{3X}), -(h/2 - d_{3X}) < z_X \leq -(h/2 - d_{3X} - d_{4X}), -(h/2 - d_{3X} - d_{4X}) < z_X < h/2 - d_{3X} - d_{4X}, h/2 - d_{3X} - d_{4X} < z_X \leq h/2 - d_{3X},$ and $z_X \geq h/2 - d_{3X}$, respectively, where z_X is the distance between the center of a bead X and the walls. For all the beads, $\epsilon_{PW} = \frac{1}{8}\epsilon_{HB}$, so chosen to represent realistically the competition between protein folding and its beads' interaction with the walls. To estimate d_{3X} and d_{4X} , the energy and size parameters between the C atoms in the walls and various beads were calculated using Lorentz-Berthelot mixing rules, $\sigma_{CX} = \frac{1}{2}(\sigma_C + \sigma_X)$, and $\epsilon_{CX} = \sqrt{\epsilon_C \epsilon_X}$, where $X = N, C_\alpha, C$ and R . Then, using separate simulations (details will be given elsewhere), the interaction potential U_{CX} between different beads was estimated. The distances at which U_{CX} and its second derivative were zero were taken as d_{3X} and $d_{3X} + d_{4X}$. The results (in \AA) are, $d_{3X} = 2.85, 3.02, 3.14,$ and $3.31,$ and $d_{4X} = 0.96, 1.01, 0.98,$ and $1.12,$ for $X = N, C_\alpha, C,$ and $R,$ respectively.

We now describe how the effective diffusivity D of the proteins is computed. To do so, one must take into account the effect of the solvent on the motion of the proteins. In the previous works the solvent's effect on the proteins' motion was included only implicitly by the HP attraction between the side chains. While this might be appropriate for studying the folding, it is not so for computing D , since the solvent's viscosity η strongly and directly affects D . To explicitly include the solvent effect, we have developed the following model which, to our knowledge, is new.

We first carry out DMD simulation for a time period Δt . Suppose that the speeds of the proteins' center of mass (CM) at the beginning and end of the period Δt are, respectively, \mathbf{v}_b and \mathbf{v}_e . Since the solvent's viscosity affects the proteins' velocity in the pore, but the time

scale over which this effect is important is much different from Δt , we apply, at the end of the time period Δt , the Langevin equation (LE) to the proteins' CM to correct their velocity due to the presence of the solvent's molecules. To do so, we represent a protein as a particle with a mass m and an effective radius equal to its radius of gyration R_g . Then, the force \mathbf{F} on its CM is given by,

$$\mathbf{F} = m(\mathbf{v}_e - \mathbf{v}_b)/\Delta t. \quad (1)$$

The discretized LE is given by,

$$\Delta \mathbf{v} = \mathbf{v}_n - \mathbf{v}_b = \mathbf{F}\Delta t/m - \xi \mathbf{v}_b \Delta t/m + \Delta \mathbf{R}(\Delta t), \quad (2)$$

where, $\xi = 6\pi R_g \eta$, $\Delta \mathbf{R}$ is a Gaussian random force (with zero mean and variance $2k_B T \xi \Delta t/m^2$), and \mathbf{v}_n is the speed *after* applying the LE (acting as the \mathbf{v}_b for the next LE application). Thus,

$$d\mathbf{v} = \mathbf{v}_n - \mathbf{v}_e = -\xi \Delta t \mathbf{v}_b/m + \Delta \mathbf{R}(\Delta t), \quad (3)$$

which yields \mathbf{v}_n , the velocity of the proteins corrected for the solvent effect. The DMD simulation is then continued for another time period Δt using \mathbf{v}_n as the \mathbf{v}_b , the LE is applied again to correct the proteins' velocity at the end of the period, and so on.

We now present the results of our simulations. Consider the case of attractive interaction potential U^+ between the proteins and the pore's walls. A folded state attaches itself to the walls only through its end groups, while unfolded ones may completely attach themselves to the walls. Thus, with U^+ the decrease in the average potential energy of the unfolded states is larger than the corresponding decrease for the folded one. Hence, compared to the bulk, the unfolded states in the pore with a U^+ are more stable than the folded one, in qualitative agreement with Refs. [4,20] for spherical cavities.

Figure 1 shows a sequence of events for a protein of size $\ell = 16$ in a pore of size $h = 1.75$ nm at $T_f \simeq 0.13$. The protein changes its state from completely folded to a partially folded to an unfolded one which is completely attached to the pore's wall (frame D). Due to U^+ , the transitions occur easily and repeatedly, even after a long time. Note that, in moving from B to C, the set of deformed α -helical HBs changes, hence indicating rapid dynamics of the HB formation and deformation near T_f .

Also shown in Figure 1 are protein configurations (frames E and F with pore size $h = 1.5$ nm) for $\ell = 9$ at $T = 0.08$. In these pores, a protein of length $\ell = 9$ does not attain its native state at low T . Instead, it has a U shape with its two sides attached to the walls; it has 4 HBs, only one of which is α -helical (the native state has 5 α -helical HBs), and more of its atoms are close to the walls than those in the folded state. Although the potential energy of such unfolded states is roughly the same as one in the folded one, entropic effects which favor the unfolded states are also important. Upon further cooling at T below the apparent folding temperature T_f , the

protein becomes trapped in the U shape without enough kinetic energy to overcome the energy barrier to attain a folded state. Thus, such configurations do not represent truly folded states.

We also find that T_f decreases with the pore size, which is due to the attractive interaction energy between the protein and the walls. The decrease in T_f is indicative of the more stable unfolded states (or less stable folded state).

The opposite (namely, increasing T_f with decreasing pore size) is true if the interaction is purely repulsive, U^- . In that case, proteins are even more confined in the pores. Thus, the number of possible unfolded states and, hence, their total entropy, will be smaller [28]. But, due to its compact configuration, confinement affects the entropy of the folded state less strongly, implying that, in the presence of U^- the folded state is more stable than that in the bulk.

Figure 2 presents the average interaction energy $\langle U_{PW} \rangle$ of the proteins with the walls, computed by the weighted histogram analysis method [29]. Cooling the proteins at $T > T_f$ increases $|\langle U_{PW} \rangle|$, as well as the average $\langle n_\alpha \rangle$ of the α -helical HBs (which is, however, very small). Near T_f $\langle n_\alpha \rangle$ is nonnegligible, and the proteins can only laterally attach themselves to the walls, hence decreasing $|\langle U_{PW} \rangle|$. By lowering T further, nearly the entire α -helix is formed, and $|\langle U_{PW} \rangle|$ increases again. Thus, Figure 2 indicates that, not only does the interaction with a nanopore disturb folding, but also folding to a definite structure disturbs the proteins' interaction with the pore.

Before describing the results for the effective diffusivities, we should point out that, over the temperature range that we have simulated, the proteins resemble a prolate ellipsoid. Thus, they become elongated in very small nanopores, while they can "stand up" in larger pores, such that their ends touch the pores' walls, if they are long enough. Such configurations are also shown in Figure 1. Thus, transport in small pores may actually be faster than in larger pores, a counterintuitive, but important result. Such phenomena can complicate further delineation of the dependence of D on the various important parameters of the system.

Our simulations indicate that transport of the proteins in the xy planes (parallel to the pore's walls) is Fickian, so that, after a sufficiently long time (which depends on the proteins' length, the pore size, and U^\pm) the mean-square displacements (MSDs) of the proteins' CM vary linearly with the time, hence yielding an effective diffusivity D for the proteins. In contrast, the MSDs in the direction perpendicular to the pore's walls saturate at a finite time.

Figure 3 presents the proteins' effective diffusivity D in the xy planes, in a pore with fixed $h/R_g = 4.1$. As T increases and T_f is approached, D also increases, since the proteins' R_g decreases. Far from T_f (where R_g changes little) D varies roughly linearly with T . However, near T_f , there are strong thermal fluctuations due to which R_g

strongly varies with T . Consequently, D no longer varies linearly with T . Increasing the proteins' length decreases D , as expected.

Figure 4 presents the diffusivities for a protein of fixed length, $\ell = 16$, in four different pores, and compares the results with those in the bulk. Note that, the T_f for the bulk state and those for the pores are not the same. Therefore, due to the strong fluctuations of R_g and D in the region around T_f , the pore and bulk diffusivities cannot be directly compared. The comparison is possible mainly at temperatures far from T_f (both below and above T_f). As Figure 4 indicates, at least for the $D_{\text{bulk}} \geq D_{\text{pore}}$ (taking into account the numerical uncertainties).

The results shown in Figures 3 and 4 were for an attractive potential U^+ between the proteins and the pores' walls. Figure 5 compares the diffusivities for a protein of length $\ell = 16$ in a pore of size $h = 1.75$ nm for both attractive and repulsive interaction potentials U^\pm , and compares them with the bulk values. Generally speaking, for $T \leq T_f$ the diffusivities with U^- are larger than those with U^+ .

In our current work, we are carrying out extensive simulations for computing the effective diffusivity D as a function of the strength of the interaction potential U_{PW} between the proteins and the walls, its sign (attractive versus repulsive), and other relevant parameters. The results will be presented in a future paper.

We thank M. R. Ejtehadi, C. K. Hall, and M. D. Niray for useful discussions. The work of LJ was supported by Iranian Nanotechnology Initiative.

-
- [1] Branden, C.; Tooze, J. *Introduction to Protein Structure*; Garland Publishing: New York, 1998.
 - [2] Anfinsen, C. B. *Science* **1973**, *181*, 223.
 - [3] Klimov, D. K.; Thirumalai, D. *Phys. Rev. Lett.* **1996**, *76*, 4070.
 - [4] Mirny, L.; Shakhnovich, E. *Annu. Rev. Biophys. Biomol. Struct.* **2001**, *30*, 361.
 - [5] Lu, S.; Liu, Z.; Wu, J. *Biophys. J. BioFAST* **2006**, *105*, 071761.
 - [6] Kirschner, D. A.; Abraham, C.; Selkoe, D. J. *Proc. Natl. Acad. Sci. USA* **1986**, *83*, 503.
 - [7] Conway, K. A.; et al. *Proc. Natl. Acad. Sci. USA* **2000**, *97*, 571.
 - [8] Lynn, D. G.; Meredith, S. C. *J. Struct. Biol.* **2000**, *130*, 153.
 - [9] Thomas, J. G.; Ayling, A.; Baneyx, F. *Appl. Biochem. Biotechnol.* **1997**, *66*, 197.
 - [10] Eggers, D. K.; Valentine, J. S. *Prot. Sci.* **2001**, *10*, 250.
 - [11] Brinker, A.; et al. *Cell* **2001**, *107*, 223.
 - [12] Tagaki, F.; Koga, N.; Takada, S. *Proc. Natl. Acad. Sci. USA* **2003**, *100*, 11367.

- [13] Bickerstaff, G. F. *Immobilization of Enzymes and Cells*; Humana Press: Totowa, NJ, 1997.
- [14] Lei, C.; et al. *J. Am. Chem. Soc.* **2002**, *124*, 11242.
- [15] Dadvar, M.; Sahimi, M. *Chem. Eng. Sci.* **2003**, *58*, 4935.
- [16] Avramescu, M.-E.; Borneman, Z.; Wessling, M. *Biotechnol. Bioeng.* **2003**, *84*, 564.
- [17] Elyassi, B.; Sahimi, M.; Tsotsis, T. T. *J. Memb. Sci.* **2007**, *288*, 290.
- [18] Rosenbloom, A. J.; et al. *Biomed. Microdev.* **2004**, *6*, 261.
- [19] Ping, G.; et al. *J. Chem. Phys.* **2003**, *118*, 8042.
- [20] Cheung, M. S.; Klimov, D.; Thirumalai, D. *Proc. Natl. Acad. Sci. USA* **2005**, *102*, 4753.
- [21] Regan, L.; DeGrado, W. F. *Science* **1988**, *241*, 976.
- [22] Guo, Z.; Thirumalai, D. *J. Mol. Biol.* **1996**, *263*, 323.
- [23] Takada, S.; Luthey-Schulten, Z.; Wolynes, P. G. *J. Chem. Phys.* **1999**, *110*, 11616.
- [24] Smith, A. V.; Hall, C. K. *Proteins* **2001**, *44*, 344.
- [25] Smith, A. V.; Hall, C. K. *Proteins* **2001**, *44*, 376.
- [26] Nguyen, H. D.; Marchut, A. J.; Hall, C. K. *Prot. Sci.* **2004**, *13*, 2909.
- [27] Smith, S. W.; Hall, C. K.; Freeman, B. D. *J. Comput. Phys.* **1997**, *134*, 16.
- [28] Thirumalai, D.; Klimov, D. K.; Lorimer, G. H. *Proc. Natl. Acad. Sci. USA* **2003**, *100*, 11195.
- [29] Ferrenberg, A. M.; Swendsen, R. H. *Phys. Rev. Lett.* **1989**, *63*, 1195.

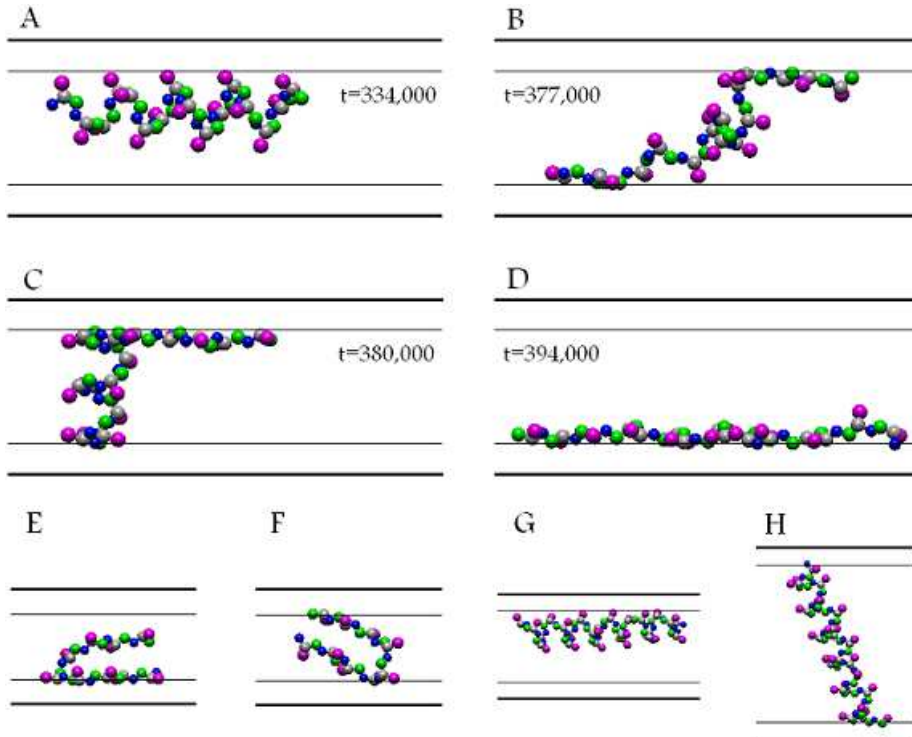


FIG. 1. Various configurations (A-D) that a protein of length $\ell = 16$ takes on in a pore at $T_f \simeq 0.13$. Blue, gray, green, and pink spheres show, respectively, the N bead, C_α , C, and the side chains. In between the walls and the thin lines at a distance d_3 , $U_{PW} = \infty$, beyond which the U^+ acts for a distance d_4 . Times t are in ps. Frames E and F show a short protein (lipid) with $\ell = 9$ that has not reached its native state. Frames G and H show the configurations of a protein parallel and perpendicular to the walls.

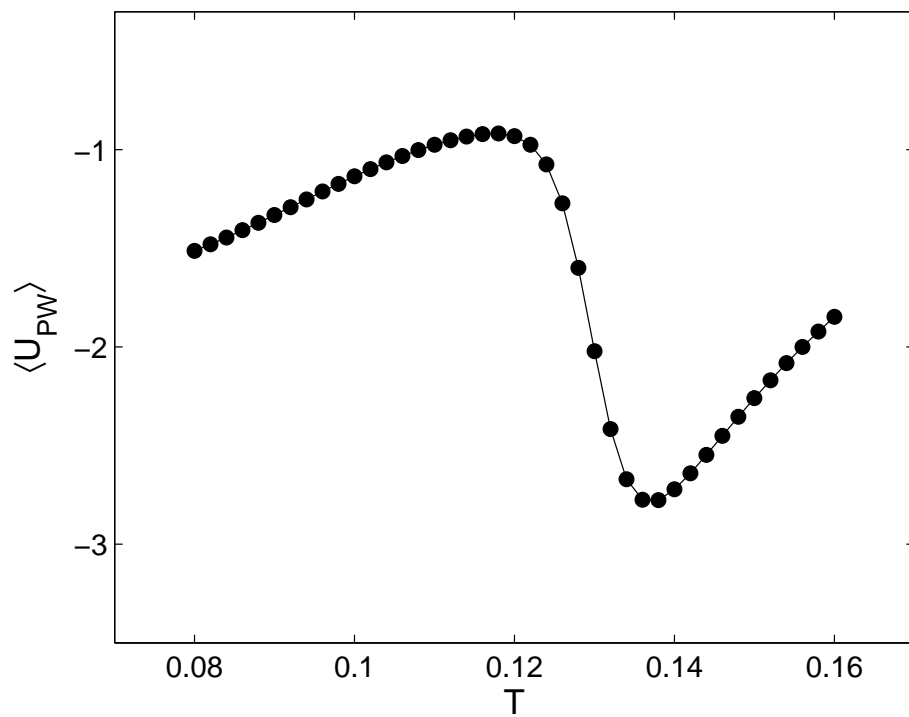


FIG. 2. The average interaction energy $\langle U_{PW} \rangle$ for a pore of size $h = 1.75$ nm and protein of length $\ell = 16$.

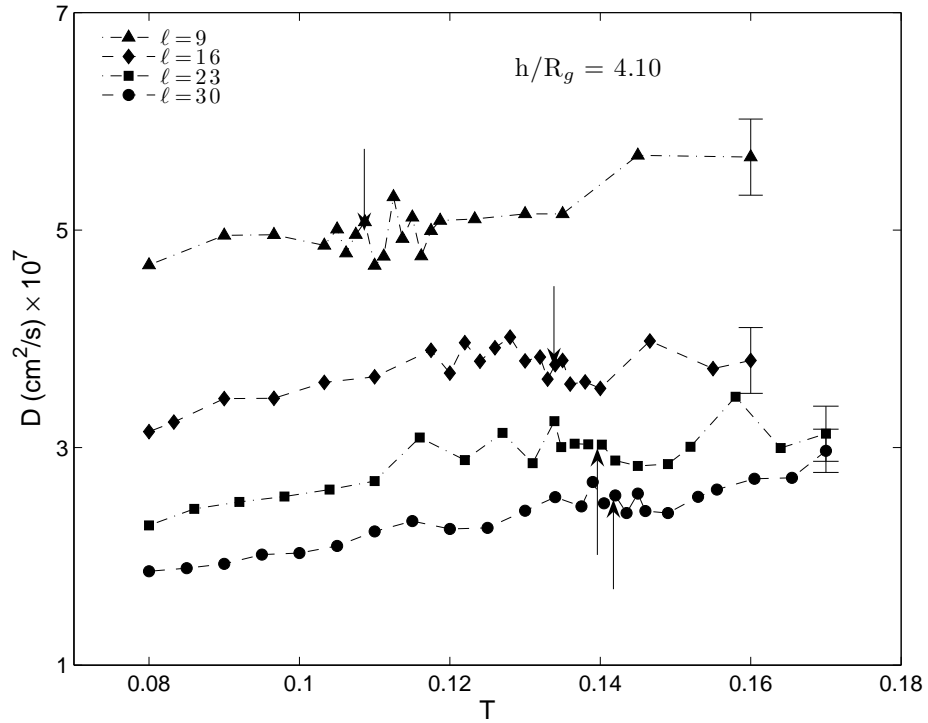


FIG. 3. Dependence of the effective diffusivity D on the temperature T for various protein length ℓ , in a pore with $h/R_g = 4.1$. Arrows indicate the location of the folding temperature T_f .

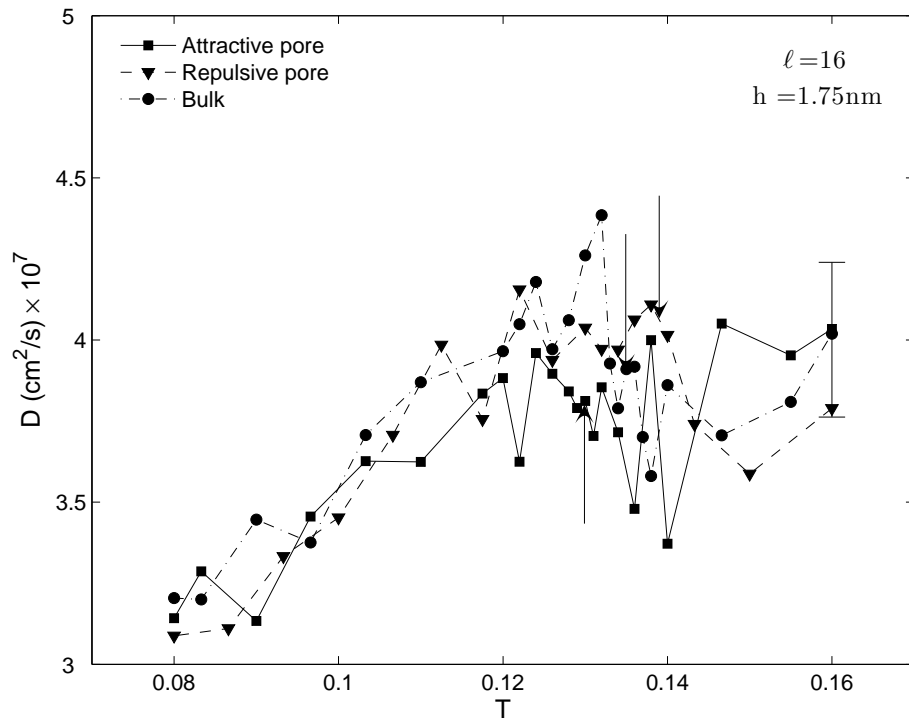


FIG. 5. Comparison of the effective diffusivities in a pore with attractive and repulsive interactions between the proteins and the pore's walls. The arrows indicate the location of T_f .